Circulating Jet for Enhancing the Mass Transfer in a Gas-liquid Stirred Tank Reactor

Lei Wang and Xiao Xu

School of Mechanical and Power Engineering, East China University of Science and Technology, Shanghai, 200237, China

Hualin Wang and Honglai Liu

State Key Laboratory of Chemical Engineering, East China University of Science and Technology, Shanghai, 200237, China

Qiang Yang*

State Environmental Protection Key Lab of Environmental Risk Assessment and Control on Chemical Process, East China University of Science and Technology, Shanghai, 200237, China

* Corresponding author at: East China University of Science and Technology,130 Meilong Road, Shanghai 200237, PR China.

E-mail address: qyang@ecust.edu.cn (Q. Yang).

A gas-liquid stirred tank reactor (STR) has some problems, such as low mass transfer efficiency, high exhaust gas oxygen concentration, and low product conversion rate, due to limitations of stirring speed and input power. This article proposes a method to enhance the gas-liquid mass transfer in a STR using circulating jet internals. It summarizes the change law of bubble size distribution, overall gas holdup, gas-liquid volumetric mass transfer

coefficient and unit volume power before and after adding circulating jet internals. When a circulating jet is added, the average bubble size in the reactor is reduced to 1.26 mm, and the overall gas holdup is increased to 8.23%, which is an increase of 3.62 times of the original STR. The gas-liquid volumetric mass transfer coefficient is increased to 0.05556 s^{-1}, which is 4.84 times of the original STR. The unit volume power is increased by only 1.4 times. These data provide references for the design and scale-up of new jet STRs.

Keywords: stirred tank reactor; circulating jet; bubble sauter mean diameter; gas holdup; volumetric mass transfer coefficient

Introduction

Stirred tank reactors (STRs) are widely used in wastewater treatment, pharmacy, fermentation, crystallization, and other industries due to the strong gas-liquid mixing, especially in biochemical processes[1-3]. Many scholars have studied the mass transfer coefficient and engineering scale-up of STRs. The stirring and mixing operations will expand the interfacial area between the gas and liquid phases, promote the gas and liquid dispersion, and enhance the heat transfer, mass transfer, and reaction between the phases[4-6]. Conventional scale-up approaches are not effective at maintaining similar values for the overall volumetric mass transfer coefficient inside industrial-scale and laboratory-scale STRs. STR scale-up can be accomplished when similar hydrodynamic conditions are observed in vessels of different diameter, and the increase in reactor size has a certain positive effect on the gas-liquid mass transfer coefficient[7]. This characteristic makes it a viable option for ordinary fermentation operations and other gas-liquid reactors.

The hydrodynamics in large-scale reactors are shown to be mainly a function of the

superficial gas velocity in the system[8,9]. The local fluid dynamics in a gas-liquid STR can accurately determine the flow state of the gas-liquid flow field[10,11]. Viscosity plays a major role in mass transfer rate in a stirred tank, whereas dissipated power has a minimal effect on the liquid-side mass transfer coefficient. In a shearing and crushing system, increasing the stirring power or gas flow is beneficial to increasing the overall gas holdup and volumetric mass transfer coefficient, whereas increasing the system viscosity will reduce the mass transfer[3,12,13]. For unit volume power input, similar mass transfer coefficients can be obtained in enlarged industrial vessels[14,15]. This finding confirms that a baffle-free stirred reactor should be regarded as a strong candidate for industrial applications, thus providing a viable alternative to baffled stirred tanks for all biochemical reaction processes.

In general, process efficiency of a gas-liquid STR highly depends on the degree of interfacial contacting. As the gas-liquid interfacial area per unit liquid volume changes, so do other important operating parameters such as volumetric heat and mass transfer coefficients[16]. Research on the gas-liquid-liquid macromixing phenomenon in a stirred tank shows that the gas-liquid-liquid macromixing was enhanced at high gas holdup and weakened at low gas holdup[17]. The energy-saving effect of an axial impeller on gas-liquid-liquid macromixing was better than that of a radial impeller. Using a sintered porous metal plate impeller as a bubble generator can improved the gas-liquid volumetric mass transfer coefficient k_La and gas holdup. At the same time, high shear stress was avoided, and the mixing energy consumption caused by the use of Rushton turbine impellers was reduced[1,18]. This type of bioreactor can be widely used in applications that require high oxygen, shear-sensitive microorganisms, and high-viscosity media in the biological fermentation process.

Aiming at the problems of low mass transfer efficiency, high exhaust gas oxygen concentration, and low product conversion rate in current stirred tank oxidation reactors, circulating jet internals have been developed to enhance gas-liquid stirring mass transfer technology. Such technology can increase the gas-liquid volumetric mass transfer coefficient while reducing the oxygen concentration of the tail gas and improving the product conversion rate and yield. The gas-liquid dispersion and mass transfer characteristics of circulating jet internals in an STR under different experimental conditions, including the influences of stirring speed and superficial gas velocity on BSD and the gas-liquid volumetric mass transfer coefficient in the reactor, are studied through experiments. Unit volume power also has a significant impact on the reactor development and the bubble generation process. This study uses a high-speed camera combined with industrial rigid endoscope technology to photograph the law of bubble movement inside the reactor. It utilizes MATLAB combined with image-processing software to identify the segmentation and reconstruction of bubble contours accurately, obtain bubble size, and compare the BSD, change law of overall gas holdup, gas-liquid volumetric mass transfer coefficient, and unit volume power before and after adding circulating jet internals. These data will provide a theoretical basis for the design and scale-up of new jet STRs.

The Experiment and Measurement

Experimental setup

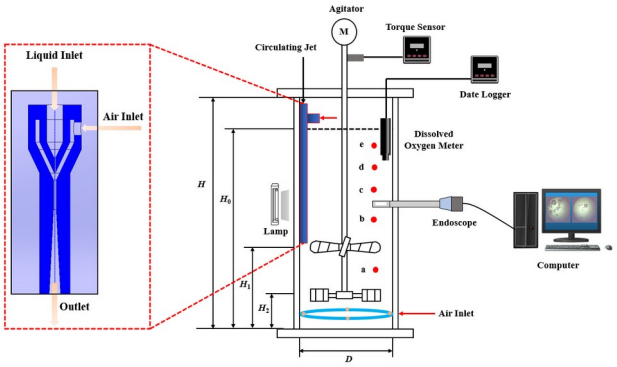

Figure 1. Experimental setup.

The experimental device is shown in Figure 1. It includes air compressor, variable frequency pump, gas mass flow meter, liquid flow meter, STR (with an inner diameter of 20 mm and a height 600 mm), ring tube bubble plate (with four distributed holes of 2 mm diameter), and circulating jet internals (with a throat diameter of 4 mm, an aspect ratio of 2, and a dispersion angle of 22.5°). Experimental testing instruments include dissolved oxygen meter, date logger, high-speed camera (AE110C), industrial rigid endoscope, and torque sensor (GB-DTSM 0.3). In the experimental process, a two-layer combined propeller adopts a radial flow propeller and an axial flow propeller to combine the advantages of each propeller type. On the one hand, the radial flow propeller is used as the bottom propeller to provide a strong shearing effect and a high gas-carrying capacity. On the other hand, the use of axial flow paddles as the upper paddles provides improved circulation in the tank, enhances the mixing effect, and reduces power consumption. The geometric parameters of the gas-liquid STR are shown in Table 1.

Table 1. Geometric parameters of the STR

Parameter	Symbol	Unit	Numerical value
Reactor height	H	mm	600
Reactor diameter	D	mm	200
Liquid level height	H_0	mm	500
Upper oar height	H_1	mm	20
Upper paddle diameter	D_1	mm	120
Bottom oar height	H_2	mm	20
Bottom oar diameter	D_2	mm	160
Installation height of the gas distributor	D_3	mm	100
Aperture of the loop distributor	d_s	mm	2
Angle between the aperture and horizontal plane of the loop distributor	θ	º	30

Bubble Measurement and Image Processing

An image of the gas-liquid multiphase flow is captured using a high-speed camera (AE110C) combined with a new vision probe industrial rigid endoscope (Olympus Borescope), and the frame rate is set to 400 frames per second. Photron FASTCAM Viewer 4.0 software is used to save one picture per frame as 400 bubble images for subsequent bubble image processing and analysis. After the bubble image is recognized by the image-processing software, the bubble contour is segmented and reconstructed using method with/without boundary extension, and parameters, such as bubble diameter and area, are obtained. The method with boundary

extension includes the following steps: 1). gray-scale image recognition; 2). bubble image segmentation; 3). overlapping bubble contour segmentation; 4). reconstruction of bubble shape with arc grouping; 5). generation of parameters, such as bubble diameter and area[10,19,20]. The image analysis processing of method with/without boundary extension is shown in Figure 2. The bubble image processed with boundary extension can well segment and reconstruct overlapping bubbles. This condition maintains the authenticity of bubble shape and greatly improve the accuracy of bubble image processing.

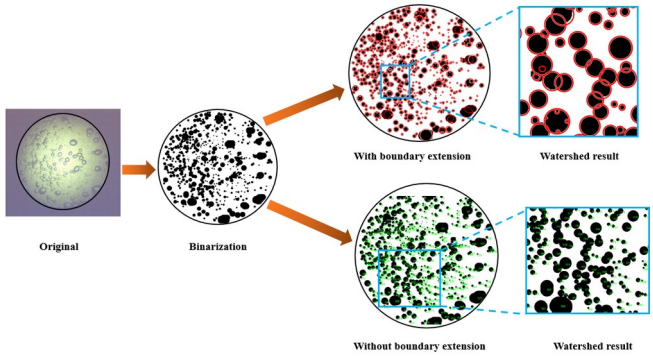

Figure 2. Bubble image analysis processing.

Figure 3 depictes the measurement values of the two bubble image-processing methods. The measurement values of method without boundary extension are relatively concentrated in a region with small bubble sizes or relatively dispersed in a region with large bubble sizes, and that is because this method has low sensitivity to identify bubble size leading to difficulty of segment and reconstruct overlapping bubbles. The measurement values of method with boundary extension used in this experiment are relatively scattered, especially with large bubble sizes, and this method has high sensitivity for bubble size boundary recognition and the resegmentation and reconstruction of bubbles. As a result, the bubble size is close to the real working condition, and the bubble measurement result is accurate.

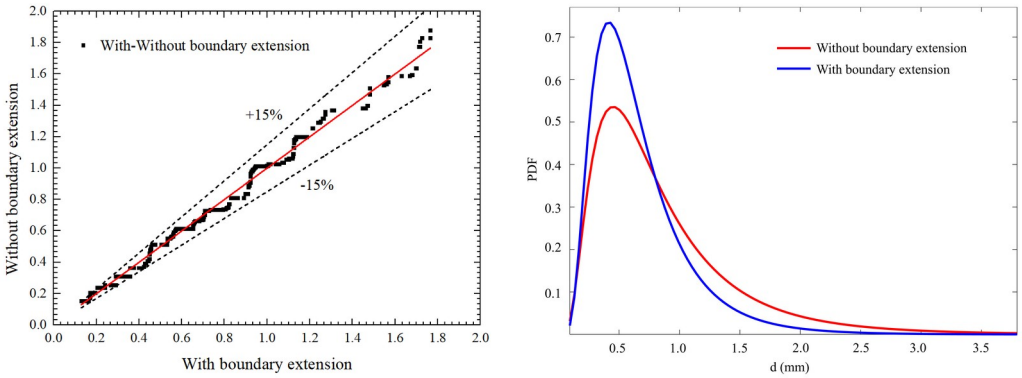

Figure 3. Comparison of two bubble image-processing results.

Performance Parameter

The overall gas holdup is an important hydrodynamic parameter of the gas-liquid STR, which directly affects the mass and heat transfer in the reactor[12]. The total gas holdup is defined as

$$\varepsilon_g = \frac{H_g - H_0}{H_g} \times 100\%, \quad (1)$$

where H_g is the liquid level of the air-sparged tank reactor, cm; H_0 is the static liquid level of the reactor, cm.

The bubbles in the gas-liquid reactor generally exist in the form of bubble groups, and the size and movement of the bubbles are relatively complicated. Thus, the size, shape, and movement characteristics of each bubble in the system are impossible to obtain accurately. On the contrary, the local properties of gas-liquid two-phase flow can accurately and intuitively reflect the gas-liquid dispersion state inside the entire reactor, and the local BSD can reflect the average bubble size at each location[21]. Therefore, the local gas-liquid properties at various points inside the reactor should be measured. In our experiments, the horizontal position points r/R=0.2,0.4,0.6,0.8, and the longitudinal position points z/R=2,3,3.5,4,4.5,5, a total of 20 positions, are measured, and the distribution of observation

points is illustrated in Figure 4.

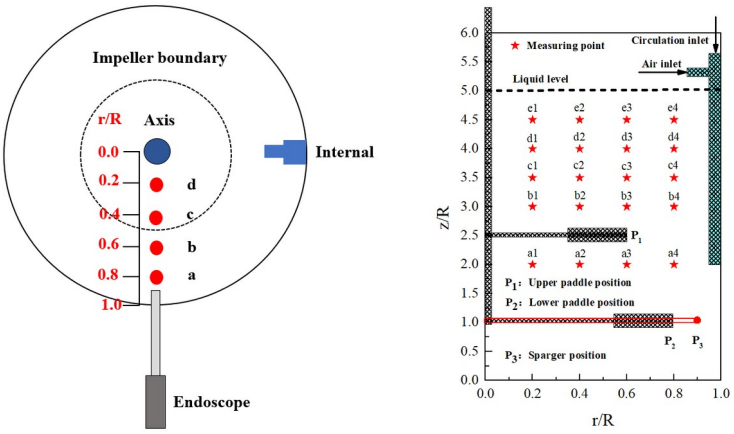

(a). Top view **(b). Longitudinal section**

Figure 4. Distribution of observation points.

The bubble Sauter mean diameter can be used to describe the local BSD characteristics. The formula for calculating the Sauter mean diameter of a group of bubbles is [9,22-24]:

$$d_{32} = \frac{\sum_{i=1}^{n}(n_i d_{ei}^3)}{\sum_{i=1}^{n}(n_i d_{ei}^2)}, \quad (2)$$

where d_{ei} is the diameter of the i-th bubble, and n_i is the number of bubbles with diameter d_{ei}.

A frequency converter and a torque sensor are used to measure the stirring speed and torque values, respectively. Owing to the existence of friction, the net torque M is obtained by subtracting the idling torque M_{Idling} from the load torque M_{Load}, then the stirring power P_1 and the unit volume power consumption P_V are calculated using the following formulas[4,25].

The net torque M:

$$M = M_{Load} - M_{Idling}, \quad (3)$$

where M_{Load} is the load torque, N·m; M_{Idling} is the idling torque, N·m.

The stirring input power P_1:

$$P_1 = 2\pi NM, \tag{4}$$

where M is the net torque, N·m; N is the stirring speed, r/min.

The circulating jet input power P_2:

$$P_2 = Q_L P_w, \tag{5}$$

where Q_L is the liquid recycle, L/min; P_W is the pressure pump, kg/cm^2.

The total input power P:

$$P = P_1 + P_2 \tag{6}$$

The unit volume power P_V:

$$P_V = P / V_{GL}, \tag{7}$$

$$V_{GL} = \frac{\pi}{4} D_0^2 \times H_2, \tag{8}$$

where V_{GL} is the liquid volume of the reactor, D_0 is the reactor diameter, and H_2 is the reactor stationary liquid level height.

The gas-liquid volumetric mass transfer coefficient is a key parameter describing the gas-liquid volumetric mass transfer and plays a vital role in the design and amplification of gas-liquid STRs[26,27]. The dynamic dissolved oxygen electrode technology is used to measure the gas-liquid volumetric mass transfer coefficient (k_La), and an appropriate gas-liquid mixing model is selected in accordance with the change in oxygen concentration in the liquid phase to fit the dissolved oxygen concentration time relationship curve[12,18,28]. The gas-liquid volumetric mass transfer coefficient k_La is calculated using the following equations[3,29]:

$$\frac{dC_L}{dt} = k_L a(C^* - C_L) \quad , \tag{9}$$

$$\ln \frac{C_L - C^*}{C_0 - C^*} = -k_L at + D^* \quad , \tag{10}$$

where C is the saturated dissolved oxygen concentration, C_0 is the dissolved oxygen concentration in a liquid at an initial time, and C_L is the dissolved oxygen concentration at a certain moment. Given that the saturated oxygen concentration is related to temperature, the temperature of k_La should be corrected in accordance with the following formula[30]:

$$(k_L a)_{20^\circ C} = \frac{(k_L a)_T}{1.022^{T-20}} \quad , \tag{11}$$

where T is the temperature under the experimental conditions, °C.

Results and Discussion

Flow Regime Distribution and Fluid Hydrodynamics

In a gas-liquid stirred reactor, three basic bubbly flow regimes are occured, namely, flooding, loading, and full recirculation[2,31]. Flooding refers that the bubbles in the reactor rarely move to the wall and gather at the reactor center. In loading regime, the bubbles move towards the wall of the reactor and are evenly dispersed on the upper part of the blade. And full recirculation denotes that the bubbles are evenly dispersed in the entire reactor, including the vicinity of the stirring blade. The transition curves of the three flow regimes are flooding-loading transition curve (F-L curve) and loading-full recirculation transition curve (L-R curve)[21,31,32]. The bubbly flow regime transition characteristics can be defined in accordance with the flow number (F_l) and the Froude Number (F_r). The flow number is the ratio of the

gas flow rate to the impeller drive flow rate, as shown in Formula (12); the Froude number is the ratio of the impeller drive acceleration to the gravity, as shown in Formula (13)[33].

$$Fl = \frac{Q_g}{ND^3}, \tag{12}$$

$$Fr = \frac{N^2 D}{g}, \tag{13}$$

where Q_g is the reactor inlet flow rate, N is the impeller speed, D is the turbine diameter, and g is the gravitational constant.

Under the conditions of stirring and bubbling in the experiment, four annular tube air volumes (10, 20, 30, and 40 L/min) and five stirring speeds (50, 100, 150, 200, and 250 rpm) are set to obtain different flow numbers Fl and Froude numbers Fr. The bubbly flow regimes under different working conditions are observed and recorded[10,16,34,35]. The bubbly flow regime distribution diagram and transition curve in this experiment are shown in Figure 5. When the gas flow rate Q_g is constant, the bubbly flow regime goes through the flooding, loading, and full recirculation states in sequence with the stirring speed increasing. When the stirring speed is constant, the Froude number Fr is determined. As the gas flow rate Q_g increases, the bubbly flow regime experiences the states of full recirculation, loading, and flooding in turn[36].

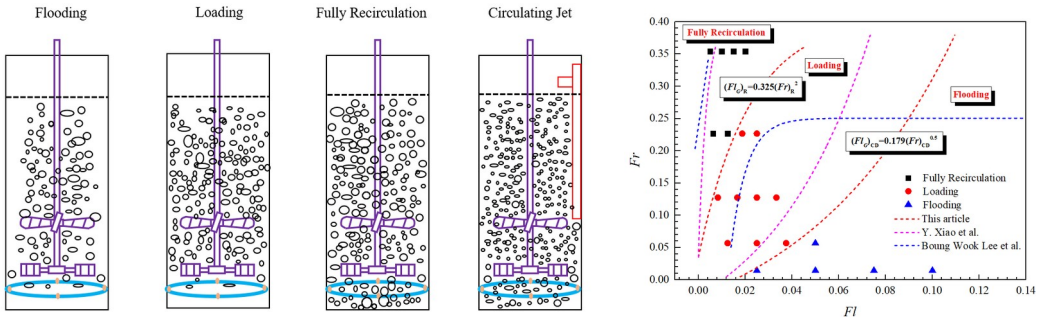

(a) **(b)**

Figure 5. Distribution of different bubbly flow regimes and transition curves. (a) Theoretical distribution diagram of different bubbly flow regimes. (b) Transition curve of the distribution of bubbly flow regimes.

The bubbly flow regime transition curve has important guiding significance for the development of STR. The gas-liquid dispersion state affect s the bubble residence time and BSD in the reactor, thereby determining the mass transfer performance and product conversion rate of the reactor. In accordance with the distribution of the bubbly flow regime transition curve shown in Figure 5(b), the transition state equations can be obtained as follows:

F-L curve: $(Fl_G)_{CD} = 0.179(Fr)_{CD}^{0.5}$ (14)

L-R curve: $(Fl_G)_R = 0.325(Fr)_R^2$ (15)

For the bubbly flow regime distribution in the experiment, uniform gas-liquid dispersion with loading and full recirculation is generally selected. A low stirring speed cannot provide the turbulent kinetic energy required for the complete dispersion of the gas and liquid. A high intake air volume provides a large bubble size and reduces the bubble residence time. Therefore, the experiment in the loading and full recirculation state will be conducive to the study of BSD and gas-liquid mass transfer efficiency.

BSD

Bubble diameter is an important characteristic of the gas-liquid STR, and it has a direct impact on the overall gas holdup and mass transfer coefficient of the reactor[37]. The change law of the bubble Sauter mean diameter at position d_3 (4-0.6) before and after adding the

circulating jet is displayed in Figure 6. The BSD in the original STR is greatly affected by the stirring speed, and the BSD range is wide. The bubble Sauter mean diameter is the largest at 100 rpm, which is 3.28 mm. While it is the smallest at 200 rpm, which is 2.72 mm. When adding the self-priming of the circulating jet, the BSD is greatly reduced by the stirring speed, and the BSD range is narrow. The bubble Sauter mean diameter is the largest at 50 rpm, which is 1.34 mm. When the stirring speed is increased to 150 rpm, the bubble Sauter mean diameter is the smallest, which is 1.17 mm. The bubble sizes of the STR and circulating jet are shown in Table 2.

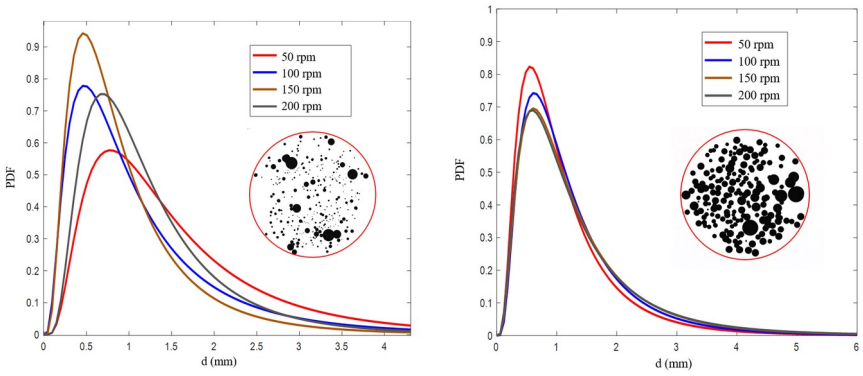

(a) Without circulating jet **(b) With circulating jet**

Figure 6. Bubble Sauter mean diameter before and after adding the circulating jet (annular tube air volume: 20 L/min; jet air intake volume: 10 L/min; z/R=4; r/R=0.6).

Table 2. Bubble sizes of the STR and circulating jet

Stirring speed	50	100	150	200
d_1/(mm, without circulating jet)	2.87	3.28	3.09	2.72
d_2/(mm, with circulating jet)	1.34	1.23	1.17	1.28

Figure 7 describes the BSD in the reactor before and after adding the circulating jet. For the initial STR (with a stirring speed of 100 rpm and an annular tube air volume of 20 L/min), the higher the position in the axial height is, the larger the bubble size will be. The smallest

bubble size, which is 1.11 mm, exists at position b_4, while the bubble size at e_2, which is 3.36 mm, is the largest. The bubble Sauter mean diameter is generally reduced when adding the circulating jet, and the BSD is uniform. The bubble size decreases when the air intake is 10 L/ min. The minimum bubble size is 0.75 mm, which is located at point a_4, and the maximum bubble size is 1.38 mm, which is located at point e_1. The bubble size increases in the bubble stirred reactor as it approaches the reactor center. The bubbles are likely to accumulate in the middle of the reactor, which increases the probability of bubbles coalescing and the bubble size. The bubble size is generally reduced after the jet air intake is increased, and the BSD is uniform. The circulating jet can generate small-scale bubbles while increasing the gas-liquid turbulence intensity and the bubble breaker rate. Therefore, the bubble size is small and evenly distributed throughout the reactor.

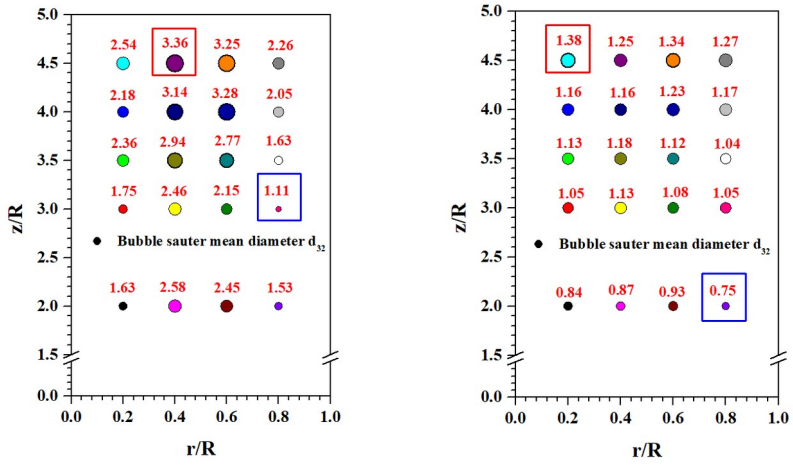

(a) STR. **(b) Circulating jet air intake at 10 L/min.**

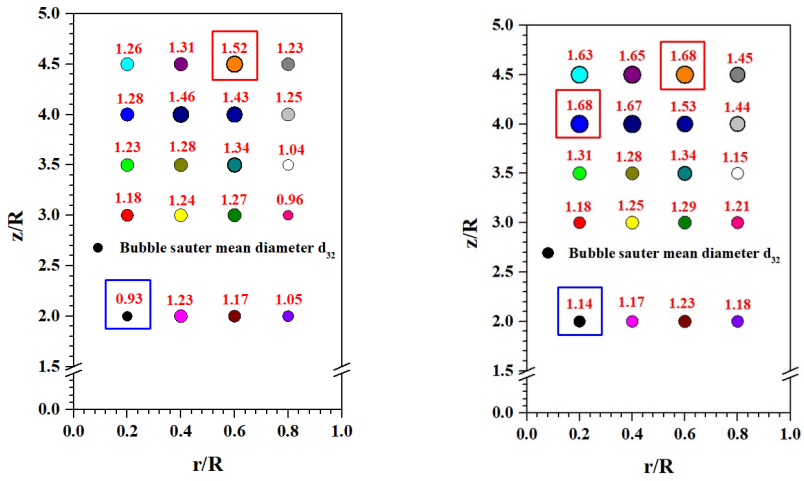

(c) Circulating jet air intake at 20 L/min. (d) Circulating jet self-priming.

Figure 7. BSD before and after adding the circulating jet (Stirring speed at 100rpm and annular tube air volume at 30 L/min).

Overall Gas Holdup

Figure 8 summarizes the change law of the overall gas holdup of the reactor before and after adding a circulating jet. For the initial STR, the gas holdup is increased from 1.23% to 3.38%, and the average gas holdup is 2.27% under four stirring speeds and three annular tube air volumes. This result is similar to those of previous studies on STR. After adding the circulating jet, the gas holdup of the reactor is greatly improved. When the intake air volume is 10 L/min, the gas holdup increases from 5.34% to 6.83%, and the average gas holdup is 6.11%, which is 2.69 times that of the initial STR. When the inlet air volume is 20 L/min, the gas holdup increases from 7.54% to 8.79%, and the average gas holdup is 8.23%, which is 3.62 times that of the initial STR. Therefore, adding a circulating jet can considerably increase the overall gas holdup of the stirred bubble reactor. From Subsection 3.2, the circulating jet can increase the overall gas holdup of the reactor by reducing the bubble diameter and improving the BSD.

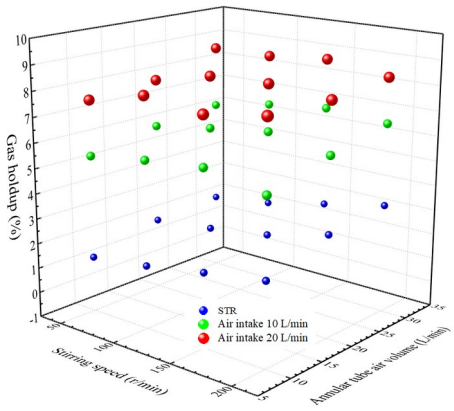

Figure 8. Change in the overall gas holdup of the reactor before and after adding a circulating jet.

In the case of the same impeller diameter, power input and superficial gas velocity are important factors affecting the overall gas holdup of the reactor[2,25,38]. The empirical correlation in the literature is expressed as follows:

$$\varepsilon = \alpha P_V^{\beta} v_s^{\gamma} . \tag{16}$$

Figure 9 depicts the variation in the overall gas holdup of the gas-liquid STR with the unit volume power and superficial gas velocity before and after increasing the circulating jet. The gas holdup of the initial stirred reactor is related to the unit volume power and superficial gas velocity, that is,

$$\varepsilon = 11.51 P_V^{0.1667} v_{s1}^{0.3724}, R^2 = 0.967 . \tag{17}$$

To illustrate the effect of the circulating jet on the overall gas holdup of the reactor, the above formula is extended to

$$\varepsilon' = \alpha' P_V^{\beta'} (v_{s1} + v_{s2})^{\gamma'} . \tag{18}$$

The obtained quantitative equation is

$$\varepsilon' = 15.66 P_V^{0.0199} (v_{s1} + v_{s2})^{0.2277}, R^2 = 0.928 , \tag{19}$$

where $0.2 \le P_V \le 7$, $0.005 \le v_{s1} \le 0.03$, and $0.002 \le v_{s2} \le 0.02$.

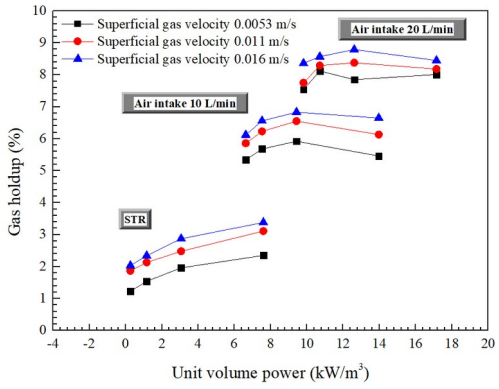

Figure 9. Relationship between the overall gas holdup of the reactor with the unit volume power and superficial gas velocity before and after increasing the circulating jet.

Gas-liquid Volumetric Mass Transfer Coefficient k_La

Figure 10 summarizes the change in the gas-liquid volumetric mass transfer coefficient k_La of the reactor before and after increasing the circulating jet. For the initial STR, the gas-liquid volumetric mass transfer coefficient k_La increases from 0.00479 s^{-1} to 0.01714 s^{-1}, and the average mass transfer coefficient is 0.01148 s^{-1} under the conditions of four stirring speeds and three annular tube air volumes. When adding the circulating jet, the mass transfer coefficient of the reactor is greatly improved. When the inlet air volume is 10 L/min, the mass transfer coefficient increases from 0.03297 s^{-1} to 0.04113 s^{-1}, and the average mass transfer coefficient is 0.03733 s^{-1}, which is 3.25 times that of the initial STR. With the inlet air volume increases to 20 L/min, the mass transfer coefficient increases from 0.05195 s^{-1} to 0.05689 s^{-1}, and the average mass transfer coefficient is 0.05556 s^{-1}, which is 4.84 times that of the initial STR. Therefore, adding a circulating jet has a remarkable effect on improving the volumetric mass transfer coefficient of the STR. The reason is similar to the increase in

the overall gas holdup. The circulating jet provides high-intensity turbulent kinetic energy while generating small-scale bubbles and uniform BSD. This condition is conducive to increasing the turbulence of the gas-liquid interface and the interfacial area of the gas-liquid, thus increasing the gas-liquid volumetric mass transfer coefficient.

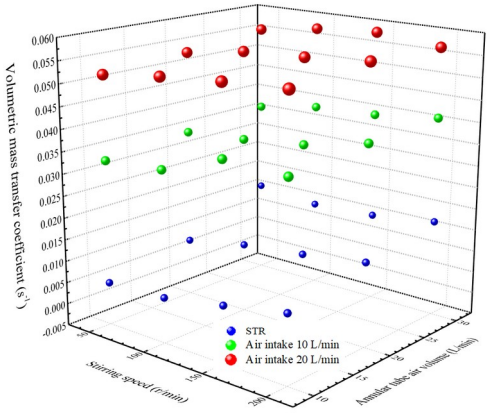

Figure 10. Change in volumetric mass transfer coefficient k_La before and after adding a circulating jet.

Similarly, when the impeller diameter is the same, the power input and superficial gas velocity are important factors affecting the gas-liquid volumetric mass transfer coefficient of the reactor[7,14,18,35]. The empirical correlation formula in the literature is

$$k_L a = C_s v_{s1}^{\alpha} P_V^{\beta} \quad (20)$$

Figure 11 depicts the variation in the gas-liquid volumetric mass transfer coefficient of the gas-liquid STR with unit volume power and superficial gas velocity before and after increasing the circulating jet. The gas-liquid volumetric mass transfer coefficient of the STR and the unit volume power and superficial gas velocity are related as shown as follows:

$$k_L a = 0.477 v_{s1}^{0.368} P_V^{0.452}, R^2 = 0.946 \quad (21)$$

To illustrate the influence of circulating jet on the gas-liquid volumetric mass transfer coefficient, the above formula is extended to

$$k_L a = C_s' (v_{s1}+v_{s2})^{\alpha'} P_V^{\beta'} \tag{22}$$

The obtained quantitative equation is

$$k_L a = 1.031(v_{s1}+v_{s2})^{1.014} P_V^{0.067}, R^2 = 0.959, \tag{23}$$

where $0.2 \le P_V \le 7$, $0.005 \le v_{s1} \le 0.03$, and $0.002 \le v_{s2} \le 0.02$.

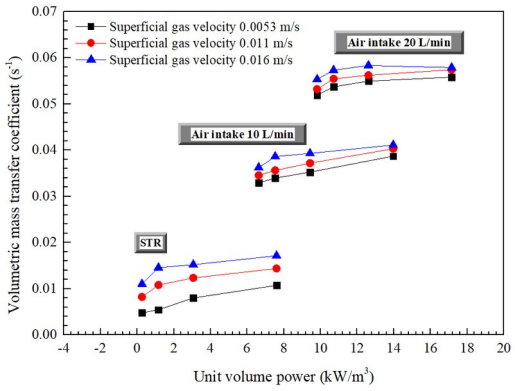

Figure 11. Relationship between volumetric mass transfer coefficient and unit volume power/superficial gas velocity.

Unit Volume Power

As shown in Figure 12, the unit volume power increases exponentially with the increase in stirring speed. The corresponding average unit volume power under the experimental conditions of 50-200 rpm is 0.24, 1.12, 2.92, and 7.227 kW/m^3. When the intake air volume is large, the unit volume power is slightly reduced. Increasing the intake air volume is beneficial to reducing the gas-liquid density in the reactor and the stirring resistance, thereby decreasing the power consumption of the stirring blade[39]. Therefore, stirring speed has a great impact on unit volume power, whereas blow volume has a relatively small impact. When the circulating

jet is added, the unit volume power still has an exponential increase relationship with stirring speed. The jet air intake should provide great energy input. The larger the jet air intake is, the more dispersed the gas-liquid phases, the lower the stirring power consumption, and the lower the unit volume power will be.

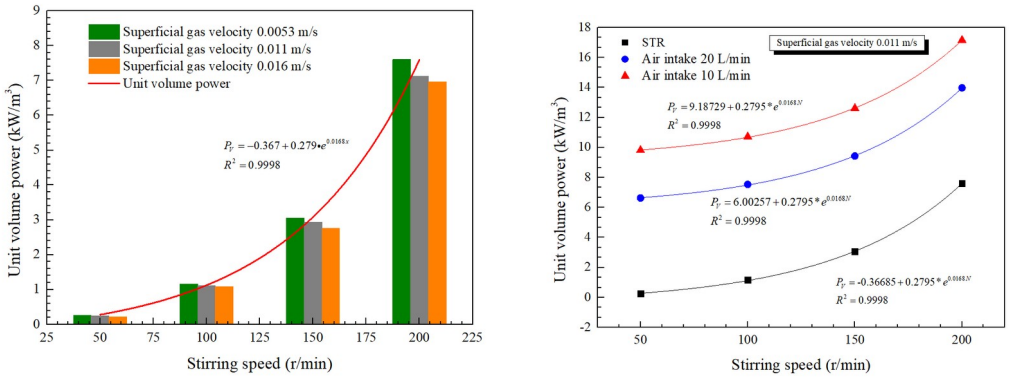

(a). STR. **(b). Before and after adding a circulating jet.**

Figure 12. Relationship between unit volume power and stirring speed.

Figure 13 plotes the effect of adding a circulating jet on the overall gas holdup and volumetric mass transfer coefficient of the reactor. With the increase in jet air intake, the overall gas holdup increases linearly, and the gas holdup can reach 14.82%, which is 3.85 times higher than that of the initial STR. The gas holdup of self- priming is 13.04%, which is 3.39 times higher than that of the initial stirred reactor. The mass transfer coefficient increases with the increase in the jet inlet until it reaches equilibrium, and the mass transfer coefficient can reach as high as 0.04214 s^{-1}, which is 2.89 times higher than that of the initial stirred bubble reactor after the jet inlet is added. At this time, the circulating jet is self-priming. Comparison of the change trend of the overall gas holdup and mass transfer coefficient of the reactor before and after the circulating jet is added shows that the circulating jet can greatly improve the overall gas holdup and mass transfer efficiency of the

reactor. The effect of the self-priming condition of the jet is also particularly good. This improvement will be applied to the study of enhancing mass transfer in a gas-liquid STR in fine chemicals. For example, for the problem of high exhaust gas oxygen concentration and low gas-liquid mass transfer efficiency in a *para*-xylene oxidation reactor, the liquid can be circulated by self-priming tail gas by adding the circulating jet self-priming process. Meanwhile, the circulating jet enhances the gas-liquid turbulent kinetic energy to produce fine bubbles for increasing the gas-liquid interfacial area. The large bubbles (d_{32}=2-3 mm) produced by bubbling are beneficial to enhancing gas-liquid turbulence, and the fine bubbles (d_{32}<1.0 mm) produced by circulating jets are beneficial to increasing the gas-liquid interfacial area. In accordance with the calculation formula of the gas-liquid volumetric mass transfer coefficient, this scale distribution will greatly enhance the gas-liquid mass transfer efficiency, thereby increasing the product conversion rate and yield.

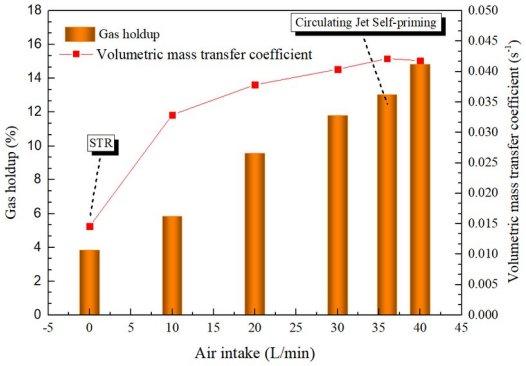

Figure 13. Effect of adding a circulating jet on the overall gas holdup and volumetric mass transfer coefficient.

Figure 14 depicts the changes in unit volume power and mass transfer coefficient under different intake air distribution ratio conditions. The intake air distribution ratio refers to the ratio of the blast volume of the ring pipe to the flow rate of the jet intake volume. Studies

have shown that with the decrease in the distribution ratio, that is, the increase in the jet air intake and the decrease in the ring blast, the gas-liquid volumetric mass transfer coefficient of the reactor gradually increases from 0.01418 s^{-1} to 0.03857 s^{-1}. The volumetric mass transfer coefficient of the complete jet air intake is 2.72 times higher than that of the complete annular air blast. The unit volume power first increases and then decreases as the distribution ratio increases. The circulating jet requires the input energy of the booster pump. Compared with the initial stirring tank reactor, the unit volume power increases from 4.16 kW/m^3 to 7.52 kW/m^3, an increase of approximately 1.81 times. When the jet air intake volume gradually increases or even replaces the blast volume of the ring pipe, the unit volume power gradually decreases. The jet air intake generates fine bubbles and reduces the gas-liquid density, thereby reducing the power consumption of the agitator. When switching to the full jet air intake condition, compared with the annular air blast, the unit volume power increases by 1.4 times, and the gas-liquid volumetric mass transfer coefficient increases by 2.72 times. Therefore, adding a circulating jet is more conducive to improving the mass transfer efficiency of the reactor than the annular air blast. At the same time, the circulating jet can self-absorb the tail gas to reduce the oxygen concentration of the tail gas, the stirring input power, and the ring bubbling volume.

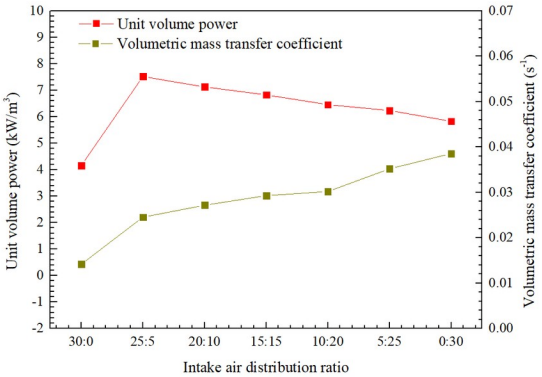

Figure 14. Influences of different distribution ratios on unit volume power and mass transfer coefficient (with a stirring speed at 100 rpm).

Industrial Application Prospect of Jet Stirred Tank Reactor

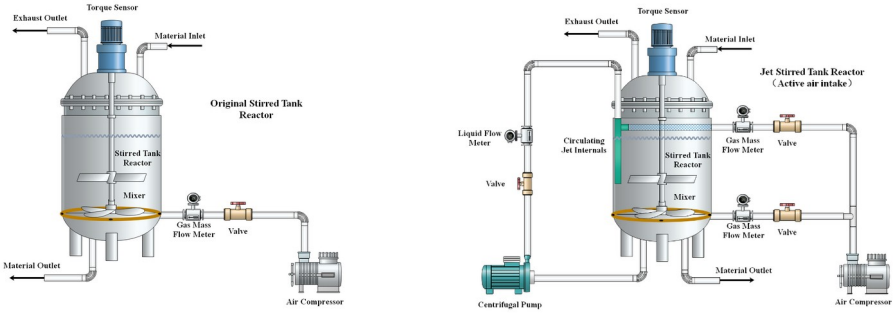

(a). Original Stirred Tank Reactor. **(b). Jet Stirred Tank Reactor (Active air intake).**

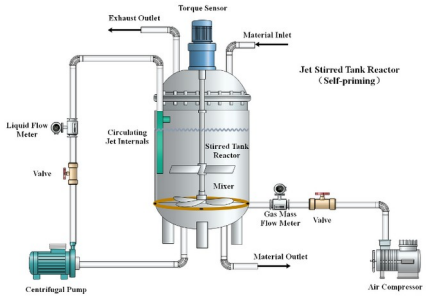

(c). Jet Stirred Tank Reactor (Self-priming).

Figure 15. Industrial Application Prospect of Jet Stirred Tank Reactor

In practical industrial applications, traditional stirred tank reactors have problems such as low mass transfer efficiency, high exhaust oxygen concentration, and high energy consumption, as shown in Figure 15(a). This is because the size of the bubbles produced by bubbling is large, which is not conducive to gas-liquid mass transfer. It is necessary to increase the stirring speed to enhance the gas-liquid turbulence and reduce the bubble size. At the same time, the power consumption increases after increasing the stirring speed, and research shows that the stirring speed has a certain limiting effect on improving the gas-liquid mass transfer. When

the stirring speed is further increased, the mass transfer efficiency does not increase in the same proportion. For the oxidation reactor, the tail oxygen concentration in the reactor needs to be strictly controlled. Therefore, it is impossible to increase the mass transfer by increasing the air flow. The original stirred tank reactor needs to be modified to increase the mass transfer and reduce the tail gas oxygen concentration. The experimental data of overall gas holdup and mass transfer coefficient are of great significance for the transformation and scale-up of stirred tank reactors. According to the research results of the intake air distribution ratio, after adopting the jet stirred tank reactor (active air intake), as shown in Figure 15(b), the bubbling air volume of the loop tube can be reduced and the jet air intake can be used to produce smaller bubbles. Furthermore, after adopting a jet stirred tank reactor (self-priming), as shown in Figure 15(c), the self-priming tail gas can generate smaller bubble sizes while reducing the oxygen concentration of the tail gas.

Conclusions

This article summarizes the law of mass transfer enhancement in a gas-liquid STR with a circulating jet. Experimental research on BSD, overall gas holdup, gas-liquid volumetric mass transfer coefficient, and unit volume power is conducted. In accordance with different bubbly flow regimes, the F-L curve: $(Fl_G)_{CD} = 0.179(Fr)_{CD}^{0.5}$ and the L-R curve: $(Fl_G)_R = 0.325(Fr)_R^2$ under experimental conditions are proposed. Comparison of the BSD in the reactor before and after adding a circulating jet shows that the circulating jet internals reduce the average bubble size in the reactor from 2.99 mm to 1.26 mm. The smaller the

circulating jet air intake is, the smaller the average bubble size will be. The BSD is more uniform after the circulating jet is added compared with that in the initial STR.

For the initial STR, the average overall gas holdup is 2.27%, and the average mass transfer coefficient is 0.01148 s^{-1}. When the circulating jet is added, the overall gas holdup and the mass transfer coefficient of the reactor is greatly improved. When the air intake is 10 L/min, the average gas holdup increases to 6.11%, which is 2.69 times that of the initial STR, and the average mass transfer coefficient is 0.03733 s^{-1}, which is 3.25 times that of the initial STR. When the intake air volume is 20 L/min, the average gas holdup increases to 8.23%, which is 3.62 times that of the initial STR, and the average mass transfer coefficient is 0.05556 s^{-1}, which is 4.84 times that of the initial STR. Adding a circulating jet considerably promote the improvement of the overall gas holdup and the mass transfer coefficient of the STR. The correlation formula between the overall gas holdup with unit volume power and superficial gas velocity is $\varepsilon' = 15.66 P_V^{0.0199} (v_{s1} + v_{s2})^{0.2277}$, $R^2 = 0.928$, where $0.2 \le P_V \le 7$, $0.005 \le v_{s1} \le 0.03$, and $0.002 \le v_{s2} \le 0.02$. While the correlation formula between the mass transfer coefficient with unit volume power and superficial gas velocity is $k_L a = 1.031 P_V^{0.067} (v_{s1} + v_{s2})^{1.014}$, $R^2 = 0.959$, where $0.2 \le P_V \le 7$, $0.005 \le v_{s1} \le 0.03$, and $0.002 \le v_{s2} \le 0.02$. Circulating jets provide high-intensity turbulent kinetic energy while generating small-scale bubbles and uniform BSD, which is beneficial to increasing the gas-liquid interface turbulence and the

gas-liquid interfacial area, thereby increasing the gas-liquid volumetric mass transfer coefficient.

The unit volume power rises exponentially as the stirring speed increases. Increasing the air intake of the circulating jet reduces the unit volume power and increases the gas-liquid volumetric mass transfer coefficient. In accordance with the study of different distribution ratios, the unit volume power increases by 1.4 times in the complete jet air intake condition compared with the stirring condition, while the gas-liquid volumetric mass transfer coefficient increases by 2.72 times. Therefore, the circulating jet flow process is expected to change the power limit to the improvement of gas-liquid mass transfer coefficient, which has important guiding significance for the design and amplification of jet STRs.

Notation

C^* the saturated dissolved oxygen concentration, $mg \cdot L^{-1}$

C_0 the dissolved oxygen concentration in a liquid at an initial time, $mg \cdot L^{-1}$

C_L the dissolved oxygen concentration at a certain moment, $mg \cdot L^{-1}$

d_b bubble diameter, mm

d_{ei} the diameter of the i-th bubble, mm

d_s aperture of the loop distributor, mm

d_{32} bubble sauter mean diameter, mm

D_0 the reactor diameter, mm

D_1 upper paddle diameter, mm

D_2 bottom oar diameter, mm

D_3 installation height of the gas distributor, mm

Fl the flow number

Fr the Froude number

g acceleration of gravity, m/s^2

H the reactor height, mm

H_g the liquid level of the air-sparged tank reactor, mm

H_0 the static liquid level of the reactor, mm

H_1 the upper oar height, mm

H_2 the bottom oar height, mm

k_La volumetric mass transfer coefficient, s^{-1}

P_V unit volume power, kW/m^3

P_W the pressure pump, kg/cm^2

Q_g the intake air flow rate, L/min

Q_L the liquid flow rate recycle, L/min

T the temperature under the experimental conditions, °C

Literature Cited

1. Jegatheeswaran S, Ein-Mozaffari F. Use of Gas Helicity as an Indicator to Evaluate Impeller Design and its Gas Holdup: Proof of Concept for the Intensification of Gas-Liquid Mixing. *Chemical Engineering and Processing - Process Intensification.* 2020;156.

2. Forte G, Alberini F, Simmons MJH, Stitt EH. Measuring gas hold−up in gas–liquid/gas-solid-liquid stirred tanks with an electrical resistance tomography linear probe. *AIChE Journal.* 2019;65(6).

3. Pino-Herrera DO, Fayolle Y, Pageot S, et al. Gas-liquid oxygen transfer in aerated and agitated slurry systems with high solid volume fractions. *Chemical Engineering Journal.* 2018;350:1073-1083.

4. Bashiri H, Bertrand F, Chaouki J. Development of a multiscale model for the design and scale-up of gas/liquid stirred tank reactors. *Chemical Engineering Journal.* 2016;297:277-294.

5. Solsvik J, Jakobsen HA. Single drop breakup experiments in stirred liquid–liquid tank. *Chemical Engineering Science.* 2015;131:219-234.

6. Jegatheeswaran S, Ein-Mozaffari F. Investigation of the detrimental effect of the rotational speed on gas holdup in non-Newtonian fluids with Scaba-anchor coaxial mixer: A paradigm shift in gas-liquid mixing. *Chemical Engineering Journal.* 2020;383.

7. Petříček R, Labík L, Moucha T, Brucato A, Scargiali F. Gas-liquid mass transfer rates in unbaffled tanks stirred by PBT: scale-up effects and pumping direction. *Chemical*

Engineering Research and Design. 2018;137:265-272.

8. Nauha EK, Visuri O, Vermasvuori R, Alopaeus V. A new simple approach for the scale-up of aerated stirred tanks. *Chemical Engineering Research and Design.* 2015;95:150-161.

9. Senouci-Bereksi M, Kies FK, Bentahar F. Hydrodynamics and Bubble Size Distribution in a Stirred Reactor. *Arabian Journal for Science and Engineering.* 2018;43(11):5905-5917.

10. Xiao Y, Li X, Ren S, Mao Z-S, Yang C. Hydrodynamics of gas phase under typical industrial gassing rates in a gas-liquid stirred tank using intrusive image-based method. *Chemical Engineering Science.* 2020;227.

11. Xiao Y, Li X, Yang C, Shen J, Mao Z-S. Particle Scattering Photography Approach for Poorly Illuminated Multiphase Reactors. II: Experimental Validation and Optimization. *Industrial & Engineering Chemistry Research.* 2018;57(25):8405-8412.

12. Liu B, Xiao Q, Sun N, Gao P, Fan F, Sunden B. Effect of gas distributor on gas-liquid dispersion and mass transfer characteristics in stirred tank. *Chemical Engineering Research and Design.* 2019;145:314-322.

13. Yamamoto T, Fang Y, Komarov SV. Mechanism of small bubble breakup in an unbaffled stirred vessel. *Chemical Engineering Science.* 2019;197:26-36.

14. Labík L, Petričříček R, Moucha T, et al. Scale-up and viscosity effects on gas-liquid mass transfer rates in unbaffled stirred tanks. *Chemical Engineering Research and Design.* 2018;132:584-592.

15. Luan D, Zhang S, Wei X, Chen Y. Study on mathematical model to predict aerated

power consumption in a gas-liquid stirred tank. *Results in Physics.* 2017;7:4085-4088.

16. Lee BW, Dudukovic MP. Determination of flow regime and gas holdup in gas–liquid stirred tanks. *Chemical Engineering Science.* 2014;109:264-275.

17. Cheng D, Cheng J, Li X, Wang X, Yang C, Mao Z-S. Experimental study on gas-liquid-liquid macro-mixing in a stirred tank. *Chemical Engineering Science.* 2012;75:256-266.

18. Li G, Li H, Wei G, et al. Hydrodynamics, mass transfer and cell growth characteristics in a novel microbubble stirred bioreactor employing sintered porous metal plate impeller as gas sparger. *Chemical Engineering Science.* 2018;192:665-677.

19. Lichti M, Bart H-J. Bubble size distributions with a shadowgraphic optical probe. *Flow Measurement and Instrumentation.* 2018;60:164-170.

20. Wang G, Li X, Yang C, Li G, Mao Z-S. New Vision Probe Based on Telecentric Photography and Its Demonstrative Applications in a Multiphase Stirred Reactor. *Industrial & Engineering Chemistry Research.* 2017;56(23):6608-6617.

21. Zhang Y, Gao Z, Li Z, Derksen JJ. Transitional flow in a Rushton turbine stirred tank. *AIChE Journal.* 2017;63(8):3610-3623.

22. Li J, Song Y, Yin J, Wang D. Investigation on the effect of geometrical parameters on the performance of a venturi type bubble generator. *Nuclear Engineering and Design.* 2017;325:90-96.

23. Han Y, Zhu J, Shen L, et al. Bubble Size Distribution Characteristics of a Jet-Stirring Coupling Flotation Device. *Minerals.* 2019;9(6).

24. Martín M, Montes FJ, Galán MA. Bubbling process in stirred tank reactors I: Agitator effect on bubble size, formation and rising. *Chemical Engineering Science.*

2008;63(12):3212-3222.

25. de Jesus SS, Moreira Neto J, Santana A, Maciel Filho R. Influence of impeller type on hydrodynamics and gas-liquid mass-transfer in stirred airlift bioreactor. *AIChE Journal.* 2015;61(10):3159-3171.

26. Jamshidzadeh M, Ein-Mozaffari F, Lohi A. Experimental Analysis of the Mass Transfer Coefficient and Interfacial Area in an Aerated Coaxial Mixing System Comprising a Non-Newtonian Solution. *Industrial & Engineering Chemistry Research.* 2020;59(49):21530-21547.

27. Li X, Li P, Zu L, Yang C. Gas-Liquid Mass Transfer Characteristics with Microbubble Aeration - I. Standard Stirred Tank. *Chemical Engineering & Technology.* 2016;39(5):945-952.

28. Garcia-Ochoa F, Gomez E. Theoretical prediction of gas–liquid mass transfer coefficient, specific area and hold-up in sparged stirred tanks. *Chemical Engineering Science.* 2004;59(12):2489-2501.

29. Ali H. Axial distributions of bubble-liquid mass transfer coefficient in laboratory-scale stirred tank with viscous Newtonian and non-Newtonian fluids. *Physics of Fluids.* 2020;32:123308.

30. Liu B, Zheng Y, Cheng R, Xu Z, Wang M, Jin Z. Experimental study on gas–liquid dispersion and mass transfer in shear-thinning system with coaxial mixer. *Chinese Journal of Chemical Engineering.* 2018;26(9):1785-1791.

31. Qiu F, Liu Z, Liu R, Quan X, Tao C, Wang Y. Gas-liquid mixing performance, power consumption, and local void fraction distribution in stirred tank reactors with a rigid-

flexile impeller. *Experimental Thermal and Fluid Science.* 2018;97:351-363.

32. Yang F, Zhou S, An X. Gas-liquid hydrodynamics in a vessel stirred by dual dislocated-blade Rushton impellers. *Chinese Journal of Chemical Engineering.* 2015;23(11):1746-1754.

33. Yang F, Sun H, Zhang C. Gas−Liquid Mixing in a Grid−Disc Impeller Stirred Tank. *Chemical Engineering & Technology.* 2020;43(7):1297-1307.

34. Shuai Y, Zhang P, Guo X, et al. Classification and identification of gas–liquid dispersion states in a jet bubbling reactor. *AIChE Journal.* 2019;66(1).

35. Kapic A, Heindel TJ. Correlating Gas-Liquid Mass Transfer in a Stirred-Tank Reactor. *Chemical Engineering Research and Design.* 2006;84(3):239-245.

36. Guan X, Li X, Yang N, Liu M. CFD simulation of gas-liquid flow in stirred tanks: Effect of drag models. *Chemical Engineering Journal.* 2020;386.

37. Cappello V, Plais C, Vial C, Augier F. Bubble size and liquid-side mass transfer coefficient measurements in aerated stirred tank reactors with non-Newtonian liquids. *Chemical Engineering Science.* 2020;211.

38. Bao Y, Wang B, Lin M, Gao Z, Yang J. Influence of impeller diameter on overall gas dispersion properties in a sparged multi-impeller stirred tank. *Chinese Journal of Chemical Engineering.* 2015;23(6):890-896.

39. Qiu F, Liu Z, Liu R, Quan X, Tao C, Wang Y. Experimental study of power consumption, local characteristics distributions and homogenization energy in gas-liquid stirred tank reactors. *Chinese Journal of Chemical Engineering.* 2019;27(2):278-285.